Structural Flexibility and Disassembly Kinetics of Single Ferritins using Optical Nanotweezers

Authors: Arman Yousefi[1], Ze Zheng[1], Saaman Zargarbashi[1], Mahya Assadipapari[1], Graham J. Hickman[2], Christopher D. J. Parmenter[3], Gabriel Sanderson[1], Dominic Craske[2], Lei Xu[1], Mohsen Rahmani[1], and Cuifeng Ying[1*]*

[1] Advanced Optics and Photonics Laboratory, Department of Engineering, School of Science and Technology, Nottingham Trent University, Nottingham NG118NS, United Kingdom

[2] School of Science and Technology, Nottingham Trent University, Nottingham NG11 8NS, United Kingdom

[3] Nanoscale and Microscale Research Centre, University of Nottingham, Nottingham NG7 2RD, United Kingdom

Corresponding Authors Email: cuifeng.ying@ntu.ac.uk; mohsen.rahmani@ntu.ac.uk

Abstract

Ferritin, a spherical protein shell assembled from 24 subunits, functions as an efficient iron storage and release system through its channels. The influence of chemicals on ferritin's conformation, dynamics, and stability remains a debated subject essential for understanding the origins of iron-related diseases in living organisms, including humans. Ascorbic Acid (Vitamin C) is one of the major elements in the human body, recognised for its association with iron-related diseases. However, its specific influence on single proteins is barely explored. In this paper, by employing optical nanotweezers using double nanohole (DNH) structures, we examined the effect of different concentrations of ascorbic acid on ferritin's conformational dynamics. The dynamics of ferritin increased as the ascorbic acid concentration approaches saturation kinetics within the ferritin core. Once the acidic conditions reach pH 2, ferritin displayed unstable fluctuations, and eventually underwent a stepwise disassembly into fragments, with each step corresponding to a transmission level in the trapping signal. We discovered four critical fragments during its disassembly pathway, which are 22-mer, 12-mer, tetramer (4-mer), and dimer (2-mer) subunits. This work further tracked the kinetics of single-molecule disassembly, demonstrating that ferritin experiences a cooperative disassembly procedure. Understanding the impact of chemicals on ferritin holds importance for disease-related implications, potential bio-applications, and their role in iron metabolism, medical treatments, and drug development.

Keywords: Single molecule, optical nanotweezers, ferritin, disassembly kinetic

Ferritin is a primary iron storage protein, consisting of a spherical cage formed by 24 identical subunits (24-mer) arranged in 3-fold and 4-fold channels on the shell.[1] Ferritin stores iron inside its cage as ferrihydrite (Fe^{3+}) core and release it as Ferrous iron (Fe^{2+}) whenever the biological organs need irons. Ferrous iron plays a crucial role in preventing oxidative damage to cells through its participation in the Fenton reaction, where it neutralises hydrogen peroxide and interacts with reactive oxygen species.[2,3] Various reductants can facilitate iron mobilisation from the ferritin shell through 3-fold channels.[4,5] For instance, ascorbic acid (AA) facilitates cellular metabolism and serves as a reducing agent for mobilising iron in ferritin.[6] Patients with hemochromatosis, a disorder characterised by significant iron overload, have lower ascorbate levels than normal and, therefore, require supplementation of ascorbate during chelation therapy.[7,8] High ascorbate levels can cause damage to proteins, lipids, and DNA by generating radicals via the Fenton reaction.[9] Additionally, high ascorbate concentrations can create an acidic environment, potentially impacting ferritin dynamics and iron release,[10] as ferritin is known to undergo disassembly at extreme acid conditions (*i.e.*, pH $\leq$ 2). The disassembled ferritin can reassemble at higher pH due to electrostatic interactions.[11] These features make ferritin promising for bio applications like drug delivery[12,13] and imaging,[14,15] but requiring deep understanding on protein behaviour in response to different conditions.[16]

Various analytical approaches, including gel electrophoresis,[17] circular dichroism,[18] ultracentrifugation,[19] and fluorescence microscopy,[20] have revealed the reversible disassembly and assembly of ferritin in response to pH changes. The pH-dependent structural alterations and assembly kinetics of ferritin have also been demonstrated in detail using small-angle X-ray scattering (SAXS).[11] These bulk measurements, however, are limited in providing information about an average response for a protein population. Recently, using high-speed atomic force microscopy (HS-AFM) and molecular dynamic (MD) simulations, Maity *et al.* [21] observed real-time disassembly-reassembly of ferritin, showing single-molecule dynamic at acidic pH

conditions. They revealed two disassembly stages: pore formation through the 3-fold channels and subsequent fragmentation into dimers. This study offers valuable insights into subunit-subunit interactions during protein disassembly. However, certain intermediate steps and small domain movements in the disassembly process are not fully captured due to the high stiffness of the AFM cantilever.[22] Molecular Dynamic simulation, on the other hand, is restricted by its short simulation time (*i.e.*, ~nanoseconds), making it difficult to track large domain movements of biological entities accurately. Therefore, a comprehensive understanding of the dynamic and kinetics behaviour of single ferritin in its native remains challenging using these methods.

Using the plasmonic optical tweezers, our recent work demonstrated the ability of monitoring the dynamic changes of ferritin during its *in situ* iron loading.[23] Here, we extended the technique for the disassembly kinetics of single, unmodified ferritin proteins. We show that ferritin exhibits increased fluctuation amplitude at ascorbic acid concentrations when approaching the saturation concentration due to a higher amount of iron release. Additionally, we exposed ferritin to different acidic pH values, and notably, under acidic conditions at pH 2, the protein demonstrated instability and underwent stepwise disassembly. For the first time, we successfully tracked the disassembly pathway and the time duration of each intermediate fragment during disassembly. Understanding of the disassembly process of ferritin could contribute to the crucial initial step in utilising ferritin for nanotechnology-based bio applications. [12,13,16]

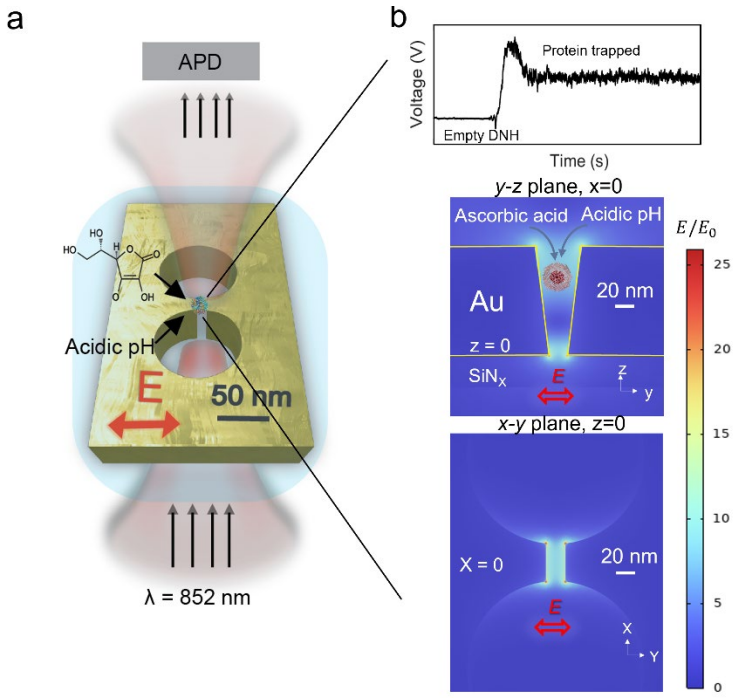

Figure 1. Concept of DNH-based optical nanotweezer with its simulated optical field distribution. (a) Schematic representation of a gold DNH positioned within the flow cell (light blue), with an 852 nm laser beam focused on the structure. Solutions of varying pH levels and different concentrations of ascorbic acid are introduced to the trapping site. The transmitted light is recorded by an avalanche photodiode (APD). (b) Top panel: transmitted optical signal demonstrating a single ferritin's trapping event. Middle and bottom panels: simulated distribution of electric field enhancement in the DNH structure in the y-z plane and x-y plane respectively.

Results and Discussion

Ascorbic acid opens pore channels of ferritin.

Figure 1a depicts the DNH structure in an aquas environment within an optical nanotweezer setup, where an 852 nm laser is focused on the structure. The localised surface plasmonic resonance generated by the gold DNH highly enhanced the optical field, as shown by the simulated field distribution in Figure 1b, with detailed simulation parameters in SI-2. The tightly confined optical field generates a strong gradient force that enables to trap a nanoparticle into the gap of the DNH.[24] The presence of the protein in the gap introduces a resonance shift, which is recorded as transmission change in the APD. Top panel of Figure 1b demonstrates a typical trapping trace, where the transmission increases upon trapping a single ferritin due to the dielectric loading. [25–27]

Ascorbic acid stimulates the conversion of ferric iron to ferrous iron, a process that results in an increased production of reactive oxygen species, specifically hydroxyl radicals.[28] Subsequently, this oxidation process gives rise to the formation of ascorbyl radicals and ferrous ions (Eq. 1). The ascorbate radical later reacts with dioxygen, leading to the regeneration of ascorbate and the generation of superoxide ion (Eq. 2). Both the superoxide and ascorbate radicals interact with ferritin, facilitating the conversion of ferric iron to ferrous iron and thereby promoting the mobilisation of iron (Eqs. 3 and 4).[29,30]

$$Fe(III) + AscH^{-} \rightarrow Fe(II) + AscH^{\bullet} \quad (1)$$

$$AscH^{\bullet} + O_2 \rightarrow AscH- + O_2^{-\bullet} \quad (2)$$

$$AscH^{\bullet} + Fe(III) \rightarrow Asc^{-} + Fe(II) \quad (3)$$

$$O2^{-\bullet} + Fe(III) \rightarrow O_2 + Fe(II) \quad (4)$$

Figure 2a illustrates the process of the ascorbic acid dissolving in water to form ascorbate. The resulting ascorbate diffuses into the ferritin core through the 3-fold channels,[31] binding to the ferric ions (Fe^{3+}) at the site of the ferroxidase centre, leading to the ferric ions reduction and eventually released from the protein.

Figure 2b displays the transmission signals of the trapped ferritin when subjected to varying concentrations of ascorbic acid. As the transmitted light intensity correlates to the conformation of the trapped protein, the root-mean-square (RMS) of the optical signals reveal the fluctuation of protein conformations.[23] The RMS of Figure 2b demonstrates an increased dynamic of ferritin within high concentrations of ascorbic acid, arising from the opening and closing of the 3-fold channels due to the permeation of ascorbate and ferrous iron. The pro-oxidant behaviour of high concentrations of ascorbic acid promotes protein's channel opening and induces increased amplitude of the transmission signal. Additionally, the loss of the ferric core after exposure to different ascorbate concentrations may contribute to the enhanced structural instability. Introducing 1 mM ascorbic acid solution to the trapped ferritin led to a 21% increase in RMS, while a concentration of 5 mM resulted in a 110% increase, indicating an accelerated rate of iron chelation and subsequent release of Fe^{2+} ions. At 10 mM, the RMS value remained higher than that of 1 mM but lower than 5 mM, exhibiting slower fluctuation in transmission signals with larger amplitude as indicated by its PDF in Figure 2d. This is attributed to the occurrence of saturation kinetics, whereby the availability of sites for interaction and surface complex formation between ascorbate and reducing agents becomes limited on the iron core, which aligns with other reported research on ferritin.[29] The repeated results confirm that the high AA concentration leads to increased dynamic motion of ferritin (Figure S2).

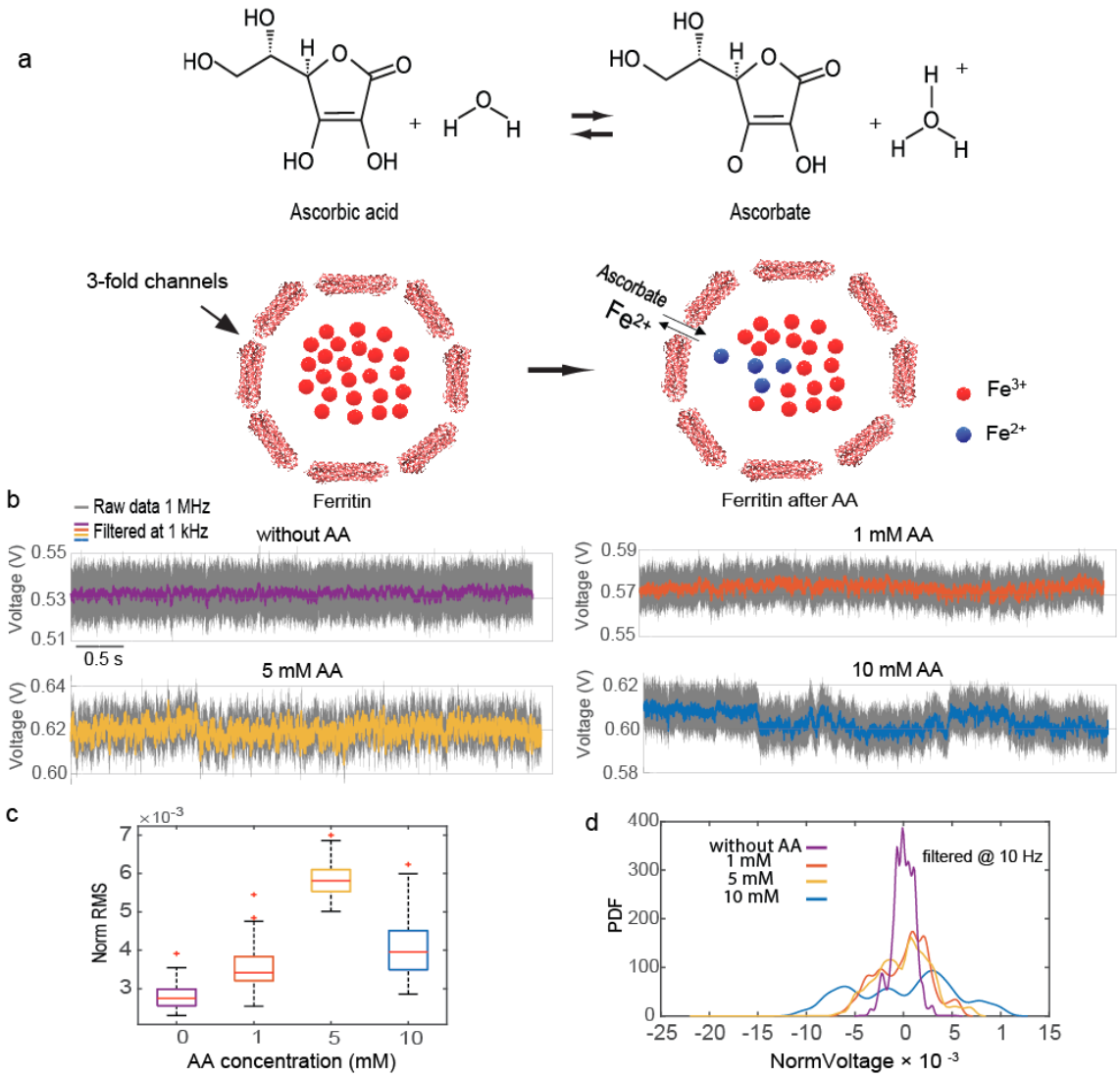

Figure 2. Effect of the ascorbic acid on the dynamic and iron releasing of ferritin. (a) Ascorbic acid dissolves in water and forms ascorbate ions. The bottom cartoons illustrate ferritin before and after exposure to ascorbic acid and how ascorbate and Fe^{2+} permeate through 3-fold channels. (b) transmission signal of DNH with trapped ferritin within different concentrations of ascorbic acid (0 mM, 1 mM, 5 mM, and 10 mM). (C) Normalised RMS of 5-second transmission signal when ferritin is trapped and introduced to different ascorbic acid concentrations. (d) Probability density function (PDF) of 5-seconds traces of a single ferritin and different ascorbic acid concentrations (filtered at 10 Hz). Data were acquired at 1 MHz and then digitally filtered at 1 kHz.

In high concentrations of ascorbic acid (1.5 M) when the solution becomes harsh acidic, we observed that ferritin underwent disassembly (Figure S3). It takes approximately 12 minutes for the ferritin to be fully disassembled and eventually escaped from the trap. During this time, the RMS value increased due to the unfolding of the ferritin channels.[21,30] Moreover, the presence of 1.5 M ascorbic acid resulted in a pH level of around 2, creating an acidic environment that further contributed to the disassembly of ferritin. To identify the impact of acidic environment on ferritin's structure, we focused on the conformational dynamics of single ferritins subjected to varying pH conditions, *in situ*.

Tracking disassembly kinetic and fragmentation of single ferritins.
To understand the effect of pH on ferritin dynamics, we trapped a single ferritin in pH 7.0 and replaced its environmental solution with acidic pH sequentially from 6.0 to 2.0 (see transmission traces in Figure 3a). The normalised RMS of the traces at pH 7.0 to pH 3.0 are relatively stable with value between 0.005 to 0.01 (Figure 3b), suggesting a stable structures within these solutions. Ferritin comprises 24 subunits categorised as heavy (H) or light (L), with the L-chain being more stable due to hydrogen bonding and salt bridges among subunits.[11,32] The equine spleen ferritin used in this work has a relatively stable structure at acidic pH due to the dominant L-chain subunits.[11,32] However, upon changing the pH to 2.0, the RMS jumps by 140%, indicating that the protein becomes highly dynamic. The mechanical instability of ferritin at pH 2.0, characterised by higher RMS values, is attributed to protein swelling, monomer rotation, and subsequent dimer movement within the 3-fold channel, leading to channel opening. [11,21,33]

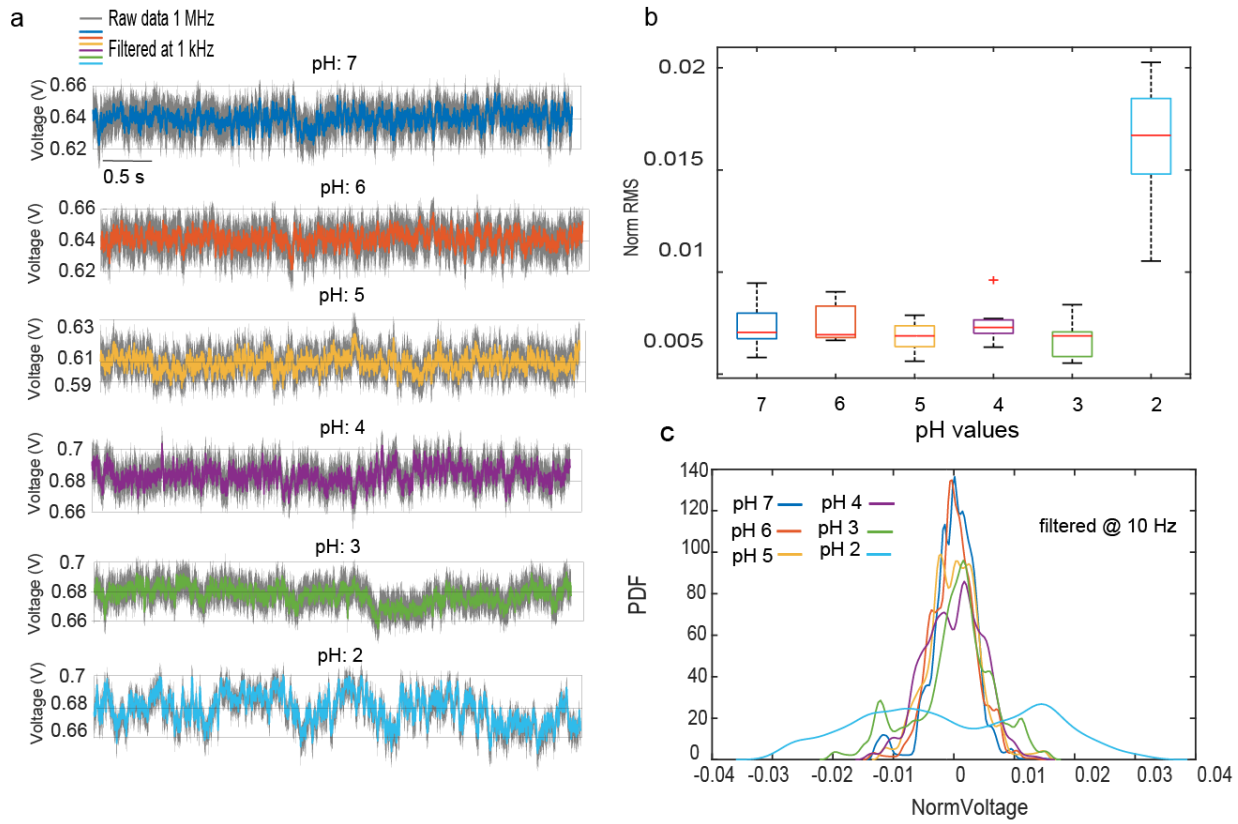

Figure 3. Conformational dynamics of a trapped ferritin exposed to solutions with different pH values.(a) Five-second transmission signals of the same ferritin exposed to solutions with pH values of 7.0, 6.0, 5.0, 4.0, 3.0, and 2.0 in sequence.(b) Normalised RMS of transmission signal for single ferritin exposed to the aforementioned pH values.(c) PDF of five-second traces corresponding to the transmission signal of single ferritin exposed to different pH values (filtered at 10 Hz). Data were acquired at 1 MHz and then Gaussian filtered at 1 kHz.

When exposed in the acidic solution for a long duration, ferritin subunits began to dissociate, causing protein disassembly. Figure 4a demonstrates the capability of our approach to track the full disassembly kinetic of ferritin about 15 minutes after introducing solution at pH 2.0. The stepwise reductions in the transmission signal in the first downfall (Figure 4b) show the step-by-step disassociation of ferritin's subunits.

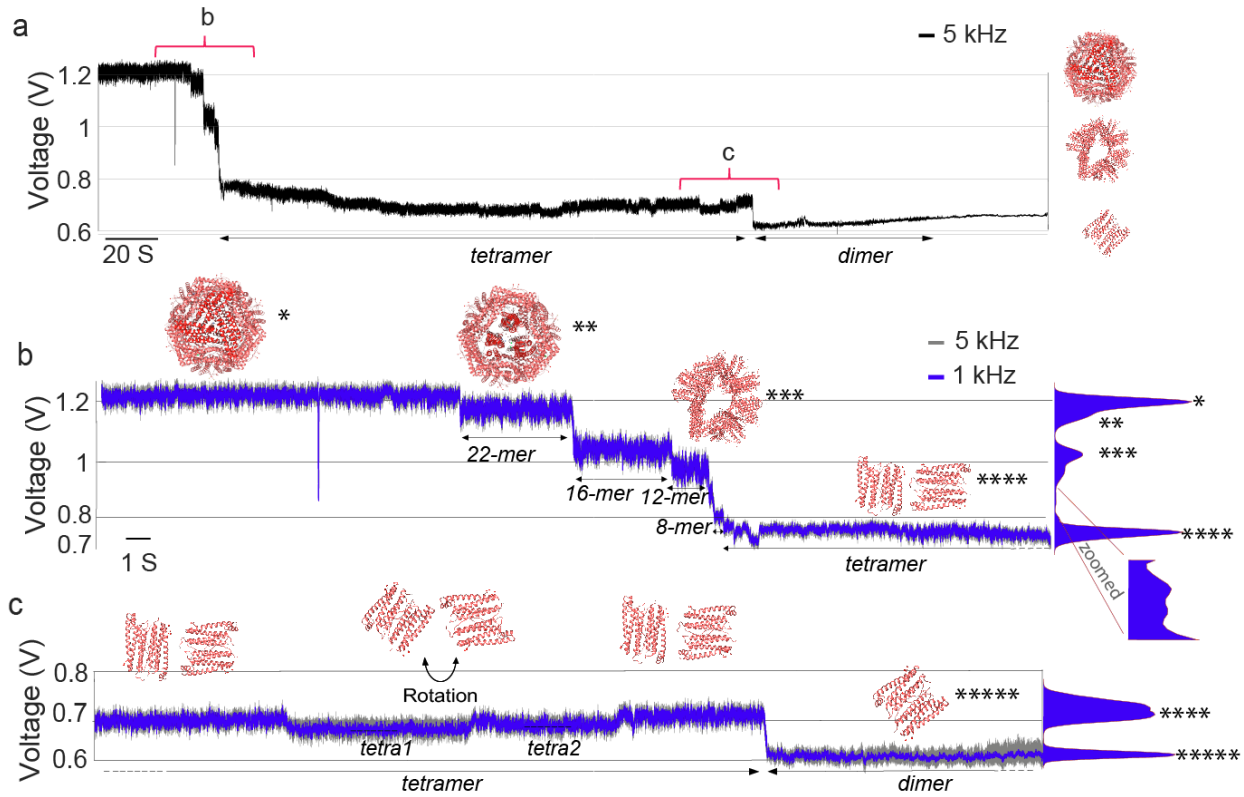

Figure 4. Disassembly process and kinetics of a single ferritin molecule into its subunits, as observed through changes in the transmission signal. (a) Full disassembly trace of a single ferritin with multiple significant drops in the transmission signal upon ferritin exposure to pH 2.0. The crystal structures on the right (PDB: 1IER) represent the structures corresponding to the transmission levels (b) An enlarged trace from panel a focusing on the oligomerisation process of ferritin. The stars mark the levels corresponding to the subunits of 20-mer, 16-mer, 12-mer, 8-mer, and tetramer, matching with the peaks of PDF on the right. (c)The second enlarged trace from panel a specifically captures the oligomerisation stage of ferritin when it reaches the tetramer stage, accompanied by the rotation of monomers and transitions into a dimeric state, again matching with the peaks of the PDF on the right.

As previously reported,[24] we expect a linear relationship between the particle volume (sphere) and the transmitted signal of DNH structures. This relationship allows us to follow the ferritin disassembly process quantitatively. When ferritin disassembles into subunits, the molecular weight of the protein remaining in the trap reduces, and consequently affects the transmission signal. The maximum transmission (V_{24mer}) during the disassembly process represents the signal from a fully assembled ferritin with 24-mer subunits, and the transmission level at which the protein is released was labelled as $V_{release}$. We linearly normalised the APD signal by taking the signal of trapped ferritin (V_{24mer}) to be 100% and the signal of empty DNH ($V_{release}$) to be 0%. By taking the sphere approximation, each subunit contributes to 4.17% of the optical signal. With this assumption, we correlated each drop of APD signal to the dissociation of a certain number of subunits. Table 1 lists the obtained mean value of APD signals of each level in Figure 4, their normalised value, and the estimated number of subunits. We first observed a drop of 10%,

corresponding to the dissociation of a dimer, leaving the ferritin to be 22-mer subunit. Further the disassembly procedure continues by reduction of the trapping signal by 30, 45, 70, 80 and 95-100% which attributes to the 16-mer, 12-mer, 8-mer, tetramer, and dimer respectively.

Table 1. Disassembly of single ferritin upon exposure to the pH 2.0

V_{mean} (mV)	$\frac{V_{Xmer} - V_{release}}{V_{24mer} - V_{release}}$	Ferritin Fragments
1200	100%	24-mer
1154	91%	22-mer
1024	68%	16-mer
943	53%	12-mer
810	29%	8-mer
730	16%	4-mer
611	7%	2-mer
645	0%	0-mer

We note that the subunits always disassociate in single or multiple dimers, due to the well-known stable 2-fold axis of the ferritin. The 24 subunits of ferritin connect to each other through the hydrogen bonding and electrostatic interactions, forming 2-, 3-, and 4-fold symmetries.[11,34,35] Among these symmetries, the two-fold axis is the most stable due to its largest number of interaction sites. Conversely, the three-fold axis is the weakest because of its fewest interaction sites. [11,35] Therefore, there is a strong chance the initial disassembly of ferritin occurs in the three-fold channels.[11] Figure 4c shows a decrease in the transmission signal, followed by two consecutive steps (tetra 1 and tetra 2), returning to the initial level (~700 mV) after 4-5 seconds for each step. As the transmission signal changes less than 1.5% and returns to the initial level, we attribute these levelled fluctuations to the rotation between dimer-dimer pairs induced by hydrogen bonding protonation at the interfaces, resulting in its shape change.[33] It is worth mentioning that this rotation process is first time tracked experimentally, thanks to the high sensitive on the polarisability of the optical nanotweezer system.[24]

Among five disassembly experiments, except two experiments where the ferritin was released from the trap before the disassembly (Figure S4), three experiments exhibited disassembly signal. These experiments are denoted as Tests 1, 2, and 3, where Test 1 corresponds to the findings depicted in Figure 4 and Table 1, and the disassembly traces of Tests 2 and 3 can be found in Figure S5. All three transmission traces exhibit distinct drops after subjecting ferritin to pH 2.0 followed by protein releasing as the signal decreasing to the baseline level eventually. These datasets allow us to decode the disassembly pathway and kinetics of single ferritin. Figure 5a identified the number of remaining subunits based on the transmission level during the disassembly process, as described by Eq. 5

$$i = \frac{V_{Xmer} - V_{release}}{V_{24mer} - V_{release}} \tag{5}$$

The high sensitivity of optical nanotweezers enables us to discover a detailed pathway of the ferritin disassembly through different fragments (Figure 5b), which is otherwise difficult for

other single-molecule techniques. We found that the disassembly of ferritin always starts with the disassociation of a dimer, forming a 22-mer assembly structure within the trap. This 22-mer fragment can go through various fragments during the disassembly. Despite of the difference in the fragmentation pathway across the three tests, certain subunits (22-mer, 12-mer, 4-mer, 2-mer) consistently maintain their integrity across all three tests, as highlighted in the Figure 5b. To the best of our knowledge, no other techniques can provide such detailed insights into ferritin disassembly.

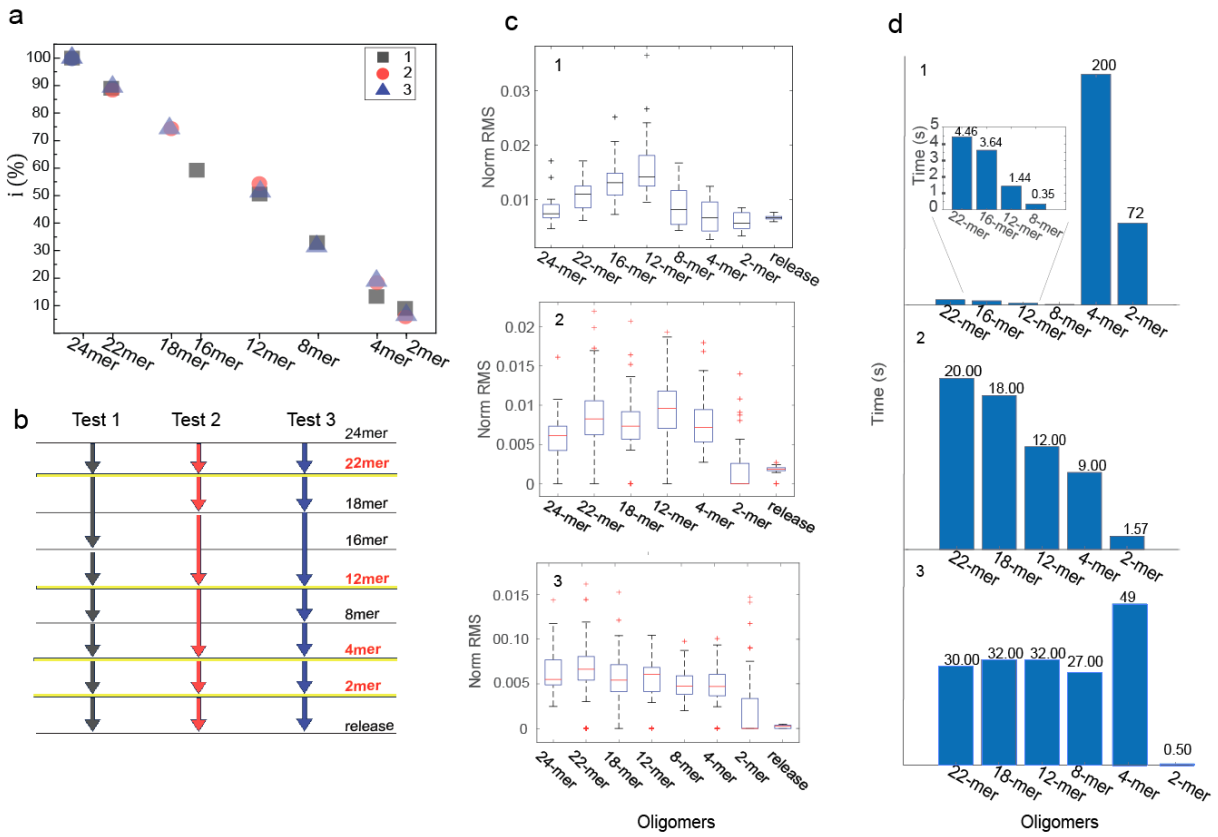

Figure 5. Single ferritin disassembly and its kinetics in three tests. (a) Number of subunits remaining in the trap during disassembly. (b) Disassembly pathways of single ferritins for three different tests. (c) Normalised RMS value of each disassembly step. (d) Dwelling time of the subunit in the trap.

The normalised RMS in Figure 5c indicates a critical point in the dynamic behaviour during ferritin disassembly, which corresponds to the 12-mer fragment. In DNH-based optical nanotweezers, the RMS value of the transmission trace decreases with the size of the trapped globular proteins.[36] In two tests (1 and 2) here, however, the RMS value increased and reached to the highest as the ferritin disassembles to a 12-mer fragment, suggesting a highly dynamic structure of 12-mer. This highly dynamic structure of 12-mer fragment arises from its large accessible areas at the subunit-subunit interfaces, leading to reduced number of hydrogen bonds between dimer-dimer interactions.[33] Additionally, the iron core inside ferritin dissolves rapidly at this stage and make the 12-mer fragment less stable. This observation is exclusively beneficial for drug delivery application of ferritin as it shows in which stage unloading occurs at a higher rate.

Previous research on the disassembly and assembly kinetics of ferritin has employed techniques like circular dichroism with SAXS, [38,39] but these methods primarily focused on the assembly process of ferritin in bulk measurement, and disassembly kinetics at the single-molecule level were not thoroughly investigated. The optical nanotweezers allow to resolve the dwelling time of each subunit during disassembly (Figure 5d). We observed a cooperative disassembly, where the disassembly of each subunit facilitates and accelerates the overall disassembly of the entire structure. This cooperative disassembly process has been demonstrated by simulation previously.[37] However, in test 3, we did not observe this cooperative reduction in dwelling times. The non-stepwise progression during the disassembly process made it difficult to identify the dwell time for each step, as shown in Figure S5b.

Conclusion

This study used the DNH structures in the optical tweezer system to investigate the impact of different concentrations of ascorbic acid and acidic pH on single ferritins *in situ*. At the single-molecule level, we observed that ferritin's dynamic gradually increases with the ascorbic acid concentration before reaching the saturation concentration (5 mM), suggesting a higher ferrous reduction from its core. When exposed to a high acid environment, *i.e.* pH 2, ferritin became highly dynamic due to the protein swelling and hydrogen bonding protonation and eventually underwent a disassembly process. We identified the number of subunits during its disassembly pathway and discovered the most essential fragments consistently existing during the disassembly, which are 22-mer, 12-mer, 4-mer, and 2-mer. The 12-mer fragment is particularly significant, as it shows the highest protein dynamics of all subunits. This study further provided the kinetic of single ferritin disassembly under acidic pH conditions, revealing cooperative disassembly kinetics. Overall, these findings on the single-molecule level provide valuable insights into the potential engineering of ferritin's structure to achieve desired functions, as reported in the existing literature.[42,43] Additionally, this work demonstrates the quantitative analytical capabilities of the optical nanotweezers for studying biomolecules, which can be applied to a wide range of protein applications in future research.

Method

Fabrication of DNH structure

The DNH structure used in this study followed the fabrication method outlined in the previous works. [23,24] Initially, 550 µm thick fused silica wafers were coated with a 30 nm silicon nitride (SiNx) layer using low-pressure chemical vapor deposition (LPCVD) at 800°C. Subsequently, a 5 nm adhesion layer of titanium (Ti) and a 100 nm layer of gold (Au) were deposited on the silicon nitride using electron beam evaporation (Leybold Optics LAB 600H) at 190°C. The silica wafers were then diced into 10 mm × 10 mm chips using a dicing machine (Disco DAD321).

To create the DNH structures within the gold film, a focused ion beam (FIB) with a gallium ion source (Zeiss Crossbeam) was employed. The DNH geometry consisted of two circles with a diameter of 160 nm, spaced 200 nm apart, and connected by a 3 nm × 40 nm rectangle. The FIB parameters were optimised with an ion beam energy of 30 kV, a beam current of 1 pA, and dwelling times of 1.25 µs for the circles and 5 µs for the rectangle. These parameters ensured DNH structures with gap sizes predominantly around 20 nm, devoid of any residual gold. The scanning electron microscopy (SEM) image of the DNH at a 20° tilt is depicted in Figure S1.

Optical nanotweezer setup

The optical components were obtained from Thorlabs, as previously described.[23] The laser was focused to a spot of approximately 1.2 µm diameter using a 60X Plan Fluor objective (Nikon, Tokyo, Japan) with a numerical aperture (NA) of 0.85. A half-wave plate was used to adjust the laser's polarisation to be perpendicular to the line connecting the centers of two holes. The power density at the DNH sample was 19 mW/µm2, resulting from the incident laser power of 32 mW before the objective. The transmitted light's intensity was measured by a silicon avalanche photodiode (APD120A, Thorlabs), which converted it into a voltage signal. The APD's voltage signal was recorded by a data acquisition card (USB-6361, NI) at a sampling rate of 1 MHz using a customised LabVIEW program.

Preparation of protein, different pH buffers, and ascorbic acid solutions

Protein solutions: We procured holo-ferritin (derived from equine spleen, F4503), along with other chemicals, from Sigma-Aldrich in the United Kingdom. For the trapping experiments, we employed 0.5 µM of ferritin in 0.1 M phosphate buffer (PB) with a pH value of 7.4.

Different pH solutions: To create solutions with varying pH levels, we adjusted the pH by adding hydrochloric acid (HCl) with a concentration of 0.1M (purchased from Fisher Scientific, product code 15697310) to deionized water. In addition to testing the pH change in deionised water, we conducted experiments in both pH 7.4 phosphate buffer (PB) and a Glycine-HCl buffer 0.1 M at pH 2.0 The Glycine-HCl buffer served as a control to assess the effects of a sudden pH shift from 7.4 to 2.0.

Ascorbic acid-buffer solution: L-Ascorbic acid (A5960) was dissolved in PB buffer (pH 7.4) at three different concentrations (1 mM, 5 mM, and 10 mM) freshly prior to each test.

Fluidic system

The flow cells used in this study are identical to those previously reported.[23,24] We produced the flow cells using a FormLab 2 printer, employing Clear V4 resin with a resolution of 50 µm (Formlabs Inc., USA). Samples in the flow cell were sealed with a cover glass measuring 0.17 mm in thickness using a two-component silicone glue (Twinsil, Picodent, Germany). The DNH sample and cover slide were separated by a 50 µm thick double-sided tape (ARcare92712, Adhesive Research, Inc.), creating a fluidic channel with a volume of 3.5 µL. A syringe pump

(Harvard Apparatus, US) controlled the flow rate and direction through a 12-port valve (Mux Distrib, Elve Flow, France). To replace the buffer after protein trapping, we introduced buffer into the flow chamber at a flow rate of 3 µL/min. Considering the internal diameter of the tubing in the flow controller system and mentioned flow rate, the different pH and ascorbic acid solutions reach the flow chamber 25 µL (6 minutes after injection) after passing through the flow controller.

Data analysis

In this study, MATLAB scripts were employed for the analysis of all presented data. Raw data underwent filtration using a zero-phase Gaussian low-pass filter with a specified cut-off frequency (1 kHz or 5 kHz) applying the filtfilt.m function. Probability density functions (PDF) were determined using the ksdensity.m function and filtered at 10 Hz. The normalised root mean square (RMS) values (Figures 2,3, and 5) were calculated by dividing the standard deviation of a 0.5-second trace by its mean value. And 0.015-second for the last figure.

Supporting Information

Scanning electron microscopy (SEM) image from the DNH sample, Optical properties of the DNH sample, Repeating test of the effect of the ascorbic acid concentrations on the signle ferritin, effect of the high concentrations of ascorbic acid on the single ferritin, non-stepwise disassembly of single ferritin upon exposure to the pH 2, Stepwise disassembly traces related to the tests 2, and 3.

Author Information

Corresponding Authors

Mohsen Rahmani- Advanced Optics and Photonics Laboratory, Department of Engineering, School of Science and Technology, Nottingham Trent University, Nottingham NG118NS, United Kingdom. Email: Mohsen.rahmani@ntu.ac.uk

Cuifeng Ying- Advanced Optics and Photonics Laboratory, Department of Engineering, School of Science and Technology, Nottingham Trent University, Nottingham NG118NS, United Kingdom. Email: cuifeng.ying@ntu.ac.uk

Authors

Arman Yousefi- Advanced Optics and Photonics Laboratory, Department of Engineering, School of Science and Technology, Nottingham Trent University, Nottingham NG118NS, United Kingdom

Ze Zheng- Advanced Optics and Photonics Laboratory, Department of Engineering, School of Science and Technology, Nottingham Trent University, Nottingham NG118NS, United Kingdom

Saaman Zargarbashi- Advanced Optics and Photonics Laboratory, Department of Engineering, School of Science and Technology, Nottingham Trent University, Nottingham NG118NS, United Kingdom

Mahya Assadipapari- Advanced Optics and Photonics Laboratory, Department of Engineering, School of Science and Technology, Nottingham Trent University, Nottingham NG118NS, United Kingdom

Graham J. Hickman- Interdisciplinary Biomedical Research Centre, School of Science and Technology, Nottingham Trent University, Nottingham NG118NS, United Kingdom

Christopher D. J. Parmenter- Nanoscale and Microscale Research Centre, University of Nottingham, Nottingham NG7 2RD, United Kingdom

Gabriel Sanderson- Advanced Optics and Photonics Laboratory, Department of Engineering, School of Science and Technology, Nottingham Trent University, Nottingham NG118NS, United Kingdom

Dominic Craske- Imaging suite, School of Science and Technology, Nottingham Trent University, Nottingham NG118NS, United Kingdom

Lei Xu- Advanced Optics and Photonics Laboratory, Department of Engineering, School of Science and Technology, Nottingham Trent University, Nottingham NG118NS, United Kingdom

Acknowledgments

This research work has been kindly supported by the Royal Society and the Wolfson Foundation. The authors appreciate the use of the NTU Imaging Suite, NTU High Performance Computing cluster Hamilton, and NTU Medical Technologies Innovation Facility (MTIF), as well as the Nanoscale and Microscale Research Centre (nmRC). M.M. acknowledges the Swiss National Science Foundation (Grant Number 200020_197239).

References

(1) Liu, X.; Theil, E. C. Ferritins: Dynamic Management of Biological Iron and Oxygen Chemistry. *Acc Chem Res* 2005, *38* (3). https://doi.org/10.1021/ar0302336.

(2) Gonciarz, R. L.; Collisson, E. A.; Renslo, A. R. Ferrous Iron-Dependent Pharmacology. *Trends in* Pharmacological Sciences. 2021. https://doi.org/10.1016/j.tips.2020.11.003.

(3) Bresgen, N.; Eckl, P. M. Oxidative Stress and the Homeodynamics of Iron Metabolism. *Biomolecules*. 2015. https://doi.org/10.3390/biom5020808.

(4) Sana, B.; Johnson, E.; Lim, S. The Unique Self-Assembly/Disassembly Property of Archaeoglobus Fulgidus Ferritin and Its Implications on Molecular Release from the Protein Cage. *Biochim Biophys Acta Gen Subj* **2015**, *1850* (12). https://doi.org/10.1016/j.bbagen.2015.08.019.

(5) Takahashi, T.; Kuyucak, S. Functional *Properties of Threefold and Fourfold Channels in Ferritin Deduced from Electrostatic Calculations*; 2003; Vol. 84.

(6) Bridges, K. R.; Hoffman, K. E. The Effects of Ascorbic Acid on the Intracellular Metabolism of Iron and Ferritin. *Journal of Biological Chemistry* **1986**, *261* (30). https://doi.org/10.1016/s0021-9258(18)67014-0.

(7) Brissot, P.; Deugnier, Y.; Le Trent, A.; Regnouard, F.; Simon, M.; Bourel, M. Ascorbic Acid Status in Idiopathic Hemochromatosis. *Digestion* **1978**, *17* (6). https://doi.org/10.1159/000198154.

(8) O'Brien, R. T. ASCORBIC ACID ENHANCEMENT OF DESFERRIOXAMINE-INDUCED URINARY IRON EXCRETION IN THALASSEMIA MAJOR. *Ann N Y Acad Sci* **1974**, *232* (1). https://doi.org/10.1111/j.1749-6632.1974.tb20588.x.

(9) Zhang, P.; Omaye, S. T. β-Carotene and Protein Oxidation: Effects of Ascorbic Acid and α-Tocopherol. *Toxicology* **2000**, *146* (1). https://doi.org/10.1016/S0300-483X(00)00160-8.

(10) Harrison, P. M. The Structure and Function of Ferritin. *Biochem Educ* **1986**, *14* (4). https://doi.org/10.1016/0307-4412(86)90203-7.

(11) Kim, M.; Rho, Y.; Jin, K. S.; Ahn, B.; Jung, S.; Kim, H.; Ree, M. PH-Dependent Structures of Ferritin and Apoferritin in Solution: Disassembly and Reassembly. *Biomacromolecules* **2011**, *12* (5). https://doi.org/10.1021/bm200026v.

(12) Palombarini, F.; Fabio, E. Di; Boffi, A.; Macone, A.; Bonamore, A. Ferritin Nanocages for Protein Delivery to Tumor Cells. *Molecules*. 2020. https://doi.org/10.3390/molecules25040825.

(13) Palombarini, F.; Masciarelli, S.; Incocciati, A.; Liccardo, F.; Di Fabio, E.; Iazzetti, A.; Fabrizi, G.; Fazi, F.; Macone, A.; Bonamore, A.; Boffi, A. Self-Assembling Ferritin-Dendrimer Nanoparticles for Targeted Delivery of Nucleic Acids to Myeloid Leukemia Cells. *J Nanobiotechnology* **2021**, *19* (1). https://doi.org/10.1186/s12951-021-00921-5.

(14) Valero, E.; Fiorini, S.; Tambalo, S.; Busquier, H.; Callejas-Fernández, J.; Marzola, P.; Gálvez, N.; Domínguez-Vera, J. M. In Vivo Long-Term Magnetic Resonance Imaging Activity of Ferritin-Based Magnetic Nanoparticles versus a Standard Contrast Agent. *J Med Chem* **2014**, *57* (13). https://doi.org/10.1021/jm5004446.

(15) Fan, K.; Gao, L.; Yan, X. Human Ferritin for Tumor Detection and Therapy. *Wiley Interdiscip Rev Nanomed Nanobiotechnol* **2013**, *5* (4). https://doi.org/10.1002/wnan.1221.

(16) Song, N.; Zhang, J.; Zhai, J.; Hong, J.; Yuan, C.; Liang, M. Ferritin: A Multifunctional Nanoplatform for Biological Detection, Imaging Diagnosis, and Drug Delivery. *Acc Chem Res* **2021**, *54* (17), 3313–3325. https://doi.org/10.1021/acs.accounts.1c00267.

(17) Smith-Johannsen, H.; Drysdale, J. W. Reversible Dissociation of Ferritin and Its Subunits in Vitro. *BBA - Protein Structure* **1969**, *194* (1). https://doi.org/10.1016/0005-2795(69)90177-9.

(18) Stefanini, S.; Vecchini, P.; Chiancone, E. On the Mechanism of Horse Spleen Apoferritin Assembly: A Sedimentation Velocity and Circular Dichroism Study. *Biochemistry* **1987**, *26* (7). https://doi.org/10.1021/bi00381a007.

(19) Harrison, P. M.; Gregory, D. W. Reassembly of Apoferritin Molecules from Subunits. *Nature* **1968**, *220* (5167). https://doi.org/10.1038/220578a0.

(20) Benni, I.; Trabuco, M. C.; Di Stasio, E.; Arcovito, A.; Boffi, A.; Malatesta, F.; Bonamore, A.; De Panfilis, S.; De Turris, V.; Baiocco, P. Excimer Based Fluorescent Pyrene-Ferritin Conjugate for Protein Oligomerization Studies and Imaging in Living Cells. *RSC Adv* **2018**, *8* (23). https://doi.org/10.1039/c8ra00210j.

(21) Maity, B.; Li, Z.; Niwase, K.; Ganser, C.; Furuta, T.; Uchihashi, T.; Lu, D.; Ueno, T. Single-Molecule Level Dynamic Observation of Disassembly of the Apo-Ferritin Cage in Solution. *Physical Chemistry Chemical Physics* **2020**, *22* (33). https://doi.org/10.1039/d0cp02069a.

(22) Mandal, S. S. Force Spectroscopy on Single Molecules of Life. *ACS Omega* **2020**, *5* (20), 11271–11278. https://doi.org/10.1021/acsomega.0c00814.

(23) Yousefi, A.; Ying, C.; Parmenter, C. D. J.; Assadipapari, M.; Sanderson, G.; Zheng, Z.; Xu, L.; Zargarbashi, S.; Hickman, G. J.; Cousins, R. B.; Mellor, C. J.; Mayer, M.; Rahmani, M. Optical Monitoring of In Situ Iron Loading into Single, Native Ferritin Proteins. *Nano Lett* **2023**, *23* (8), 3251–3258. https://doi.org/10.1021/acs.nanolett.3c00042.

(24) Ying, C.; Karakaçi, E.; Bermúdez-Ureña, E.; Ianiro, A.; Foster, C.; Awasthi, S.; Guha, A.; Bryan, L.; List, J.; Balog, S.; Acuna, G. P.; Gordon, R.; Mayer, M. *Watching Single Unmodified Enzymes at Work*. arXiv preprint arXiv:2107.06407.

(25) Kotnala, A.; DePaoli, D.; Gordon, R. Sensing Nanoparticles Using a Double Nanohole Optical Trap. *Lab Chip* **2013**, *13* (20), 4142. https://doi.org/10.1039/c3lc50772f.

(26) Zehtabi-Oskuie, A.; Bergeron, J. G.; Gordon, R. Flow-Dependent Double-Nanohole Optical Trapping of 20 Nm Polystyrene Nanospheres. *Sci Rep* **2012**, *2* (1), 966. https://doi.org/10.1038/srep00966.

(27) Pang, Y.; Gordon, R. Optical Trapping of 12 Nm Dielectric Spheres Using Double-Nanoholes in a Gold Film. *Nano Lett* **2011**, *11* (9), 3763–3767. https://doi.org/10.1021/nl201807z.

(28) Timoshnikov, V. A.; Kobzeva, T. V.; Polyakov, N. E.; Kontoghiorghes, G. J. Redox Interactions of Vitamin c and Iron: Inhibition of the pro-Oxidant Activity by Deferiprone. *Int J Mol Sci* **2020**, *21* (11). https://doi.org/10.3390/ijms21113967.

(29) Boyer, R. F.; J. McCleary, C. Superoxide Ion as a Primary Reductant in Ascorbate-Mediated Ferretin Iron Release. *Free Radic Biol Med* **1987**, *3* (6). https://doi.org/10.1016/0891-5849(87)90017-7.

(30) Badu-Boateng, C.; Naftalin, R. J. Ascorbate and Ferritin Interactions: Consequences for Iron Release in Vitro and in Vivo and Implications for Inflammation. *Free Radical Biology and Medicine*. 2019. https://doi.org/10.1016/j.freeradbiomed.2018.09.041.

(31) Jones, T.; Spencer, R.; Walsh, C.; Jone, T.; Spencer, R.; Walsh, C. Mechanism and Kinetics of Iron Release from Ferritin by Dihydroflavins and Dihydroflavin Analogues†. *Biochemistry* **1978**, *17* (19). https://doi.org/10.1021/bi00612a021.

(32) Yoshizawa, K.; Mishima, Y.; Park, S. Y.; Heddle, J. G.; Tame, J. R. H.; Iwahori, K.; Kobayashi, M.; Yamashita, I. Effect of N-Terminal Residues on the Structural Stability of Recombinant Horse L-Chain Apoferritin in an Acidic Environment. *J Biochem* **2007**, *142* (6). https://doi.org/10.1093/jb/mvm187.

(33) Li, Z.; Maity, B.; Hishikawa, Y.; Ueno, T.; Lu, D. Importance of the Subunit–Subunit Interface in Ferritin Disassembly: A Molecular Dynamics Study. *Langmuir* **2022**, *38* (3), 1106–1113. https://doi.org/10.1021/acs.langmuir.1c02753.

(34) Vedula, L. S.; Brannigan, G.; Economou, N. J.; Xi, J.; Hall, M. A.; Liu, R.; Rossi, M. J.; Dailey, W. P.; Grasty, K. C.; Klein, M. L.; Eckenhoff, R. G.; Loll, P. J. A Unitary Anesthetic Binding Site at High Resolution. *Journal of Biological Chemistry* **2009**, *284* (36). https://doi.org/10.1074/jbc.M109.017814.

(35) Lawson, D. M.; Artymiuk, P. J.; Yewdall, S. J.; Smith, J. M. A.; Livingstone, J. C.; Treffry, A.; Luzzago, A.; Levi, S.; Arosio, P.; Cesareni, G.; Thomas, C. D.; Shaw, W. V.; Harrison, P. M. Solving the Structure of Human H Ferritin by Genetically Engineering Intermolecular Crystal Contacts. *Nature* **1991**, *349* (6309). https://doi.org/10.1038/349541a0.

(36) Wheaton, S.; Gordon, R. Molecular Weight Characterization of Single Globular Proteins Using Optical Nanotweezers. *Analyst* **2015**, *140* (14), 4799–4803. https://doi.org/10.1039/C5AN00026B.

(37) Hilser, V. J.; Dowdy, D.; Oas, T. G.; Freire, E. The Structural Distribution of Cooperative Interactions in Proteins: Analysis of the Native State Ensemble. *Proceedings of the National Academy of Sciences* **1998**, *95* (17), 9903–9908. https://doi.org/10.1073/pnas.95.17.9903.

(38) Mohanty, A.; Mithra, K.; Jena, S. S.; Behera, R. K. Kinetics of Ferritin Self-Assembly by Laser Light Scattering: Impact of Subunit Concentration, PH, and Ionic Strength. *Biomacromolecules* **2021**, *22* (4). https://doi.org/10.1021/acs.biomac.0c01562.

(39) Sato, D.; Ohtomo, H.; Yamada, Y.; Hikima, T.; Kurobe, A.; Fujiwara, K.; Ikeguchi, M. Ferritin Assembly Revisited: A Time-Resolved Small-Angle X-Ray Scattering Study. *Biochemistry* **2016**, *55* (2). https://doi.org/10.1021/acs.biochem.5b01152.

(40) Zhang, Y.; Orner, B. P. Self-Assembly in the Ferritin Nano-Cage Protein Superfamily. *International Journal of Molecular Sciences*. 2011. https://doi.org/10.3390/ijms12085406.

(41) Gerl, M.; Jaenicke, R. Mechanism of the Self-Assembly of Apoferritin from Horse Spleen - Cross-Linking and Spectroscopic Analysis. *European Biophysics Journal* **1987**, *15* (2). https://doi.org/10.1007/BF00257503.

(42)King, N. P.; Sheffler, W.; Sawaya, M. R.; Vollmar, B. S.; Sumida, J. P.; André, I.; Gonen, T.; Yeates, T. O.; Baker, D. Computational Design of Self-Assembling Protein Nanomaterials with Atomic Level Accuracy. *Science (1979)* **2012**, *336* (6085). https://doi.org/10.1126/science.1219364.

(43) Chen, H.; Zhang, S.; Xu, C.; Zhao, G. Engineering Protein Interfaces Yields Ferritin Disassembly and Reassembly under Benign Experimental Conditions. *Chemical Communications* **2016**, *52* (46). https://doi.org/10.1039/c6cc03108k.